MASTER'S THESIS

Master of Science in Advanced Mathematics and Mathematical Engineering

Title: Mathematical and computational modeling of shape-morphing surfaces

Author: Nino Guzmán De la O

Advisor: Marino Arroyo Balaguer

Department: : Departament de Matemàtiques, Facultat de Matemàtiques i Estadística

Academic year : 2019-2020:

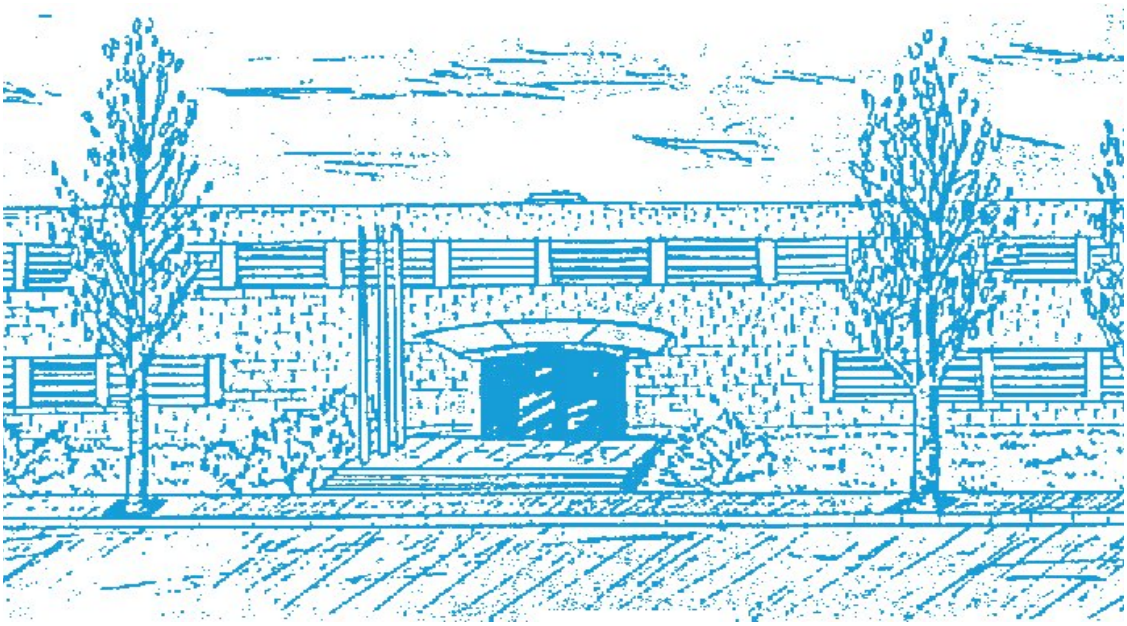

UNIVERSITAT POLITÈCNICA DE CATALUNYA
BARCELONATECH
Facultat de Matemàtiques i Estadística

To my parents Susana and Bernardino, their love and support are a continuous motivation to accomplish my goals and more important to continue improving as a person. To my sisters Susana and Stefanie and my brother Oscar for inspiring me in several ways, for supporting me in each stage of my life, for making my life unique.

To my astonishing girlfriend Stephanie, for their support and motivation to made this possible. For her patient while I was away, for been more close to me than any other moment. There are no words to acknowledge all the things you have done that made me continue with this adventure.

A ti chaparrita, hasta donde estés. Abrazo a ti y a Cheque.

Abstract

Euglenids are protists unicellular flagellates made of parallel proteinaceous strips and microtubules located underneath the plasma membrane, they exhibit a highly intriguing shape morphing mechanism that permits them to move through the media and for the feeding process. Inspired by this behaviour we develop a model to mimics the pellicle kinematics by linking the pellicle deformations and the mechanics of the rods by assuming a continuous surface made of adjacent rods. The computational model works by finding the shape configuration that minimizes the energy functional. We obtain a wide repertory of possible configurations using axisymmetric cylindrical surfaces and we obtain a reduce model for the case of inextensible rods. Additional actuation of pellicle shears should be studied to obtain a larger set of shape configurations mainly non-axisymmetrical. New numerical studies are needed to obtain smooth transitions between pairs of stable configurations.

Keywords: Euglenids, cell motility, pellicle kinematics, cell metaboly

Contents

List of Figures

Chapter 1

Introduction

When I was a kid I used to think that Leonardo da Vinci (1452-1519) was probably the major genius of all times. I mean, is there something where he was not good at? He could do all in an astonishing manner, painting, sculpting, designing, inventing. Besides his paintings, the work that is highly remembered until now, it is his ability to invent new devices. There is no doubt that a lot of his ideas came from nature. For instance, his fascination by the mechanical movement of horses and birds that lead him to design several machineries to try to make humans fly (see Fig. (1.1)).
Nowadays, artists, scientists, mathematicians and engineers in diverse range of areas, are motivated by nature, by different biological entities that triggers his creativity and curiosity, something that is called now *bioinspiration*. In this work we are going to focus our attention in the microworld, in particular, in single-cell aquatic flagellates denominated *euglenids* or *euglenoids*.

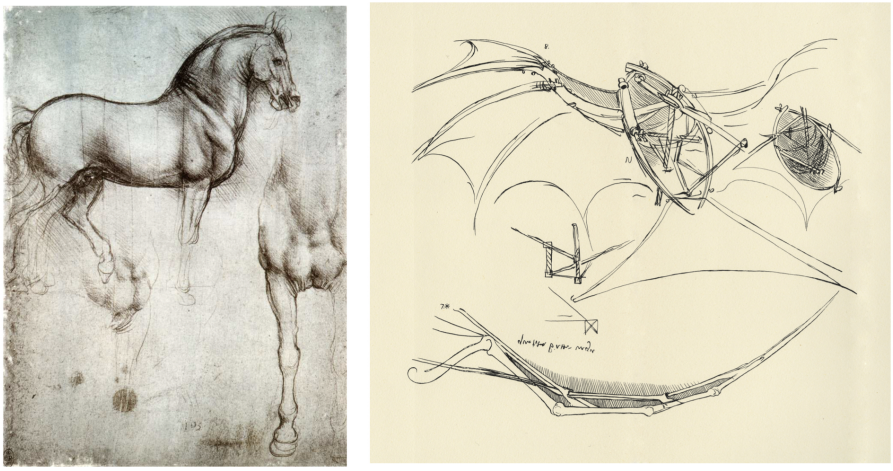

Figure 1.1: Study of horses (left) and design of flying machine (right). Images courtesy: Toronto Public Library under the license CC BY-ND 2.0.

The euglenids are protists unicellular flagellates typically they are 5–50 μm in length. They show a typical cell membrane consisting of parallel proteinaceous strips and microtubules located underneath the plasma membrane, what we called in here the pellicle (see Fig. (1.2)). They are known since the invention of the microscope [2] but some fundamental questions about their evolutionary process and their fascinating shape morphing mechanism remain open [1].
In 1977, E. M. Purcell [3] begin to explore some of this questions, mainly in how this microswimmers are able to move at such scales. From this study, the ability of euglenids to move through out the media, or *metaboly*, has been investigate it more and more [4]. This behaviour has high potential in areas such as soft robotics [5, 6], biophysics and bioengineering [7, 8, 9] but also even in mathematics [10] due to the non-linear partial differential equations that came from the relation between the pellicle deformations and the actuation shear.

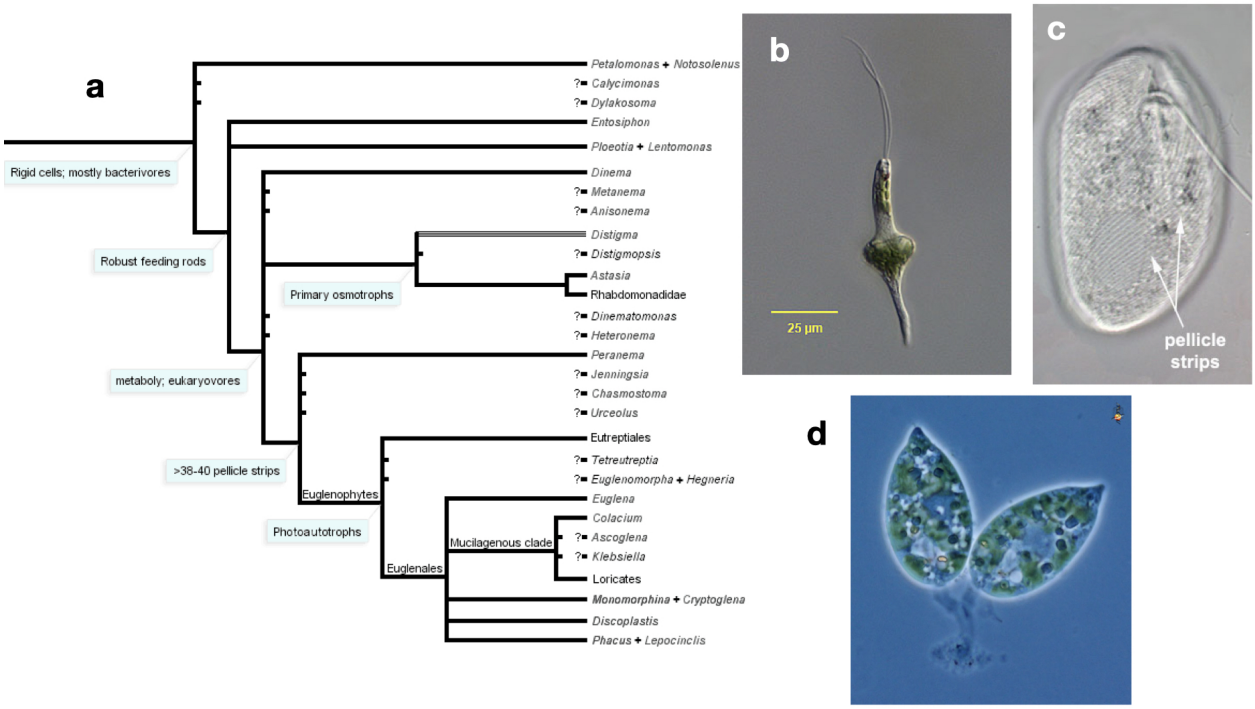

Figure 1.2: a) Phylogenetic relationships of euglenid subgroups. This media file is licensed under the license CC BY-ND 3.0., b) *Eutreptia viridis* taken from samples of freshwater stream. © William Bourland, c) aphagotrophic cell signalling the pellicle proteinaceous strips © Brian S. Leander, d) *Colacium* © 2001 D. J. Patterson and Mark Farmer. Images b), c) and d) are licensed under the license CC BY-ND 2.5.. All images belong to the The tree of life project [1].

In this work we develop a model linking the pellicle deformations and the mechanics of rods to mimics the shape deformations of the euglenids pellicle. In the chapter 2 we review some of the fundamental geometric aspects to describe a regular surface. Later on we introduce the model itself by presenting the mechanics of rods in chapter 3. A reduction of this model can be made by assuming the inextensibility of rods. At the end of the work, we provide some new lines of investigation to follow in order to understand these unicellular organisms and the life at microscale.

Chapter 2

Fundamentals of differential geometry

In this first chapter we are going to introduce the most fundamental concepts of differential geometry that will be use to model the eugelna pellicle and later on their locomotion. Mainly the review of the concepts as been done following [11] for which we kept with this notation.

2.1 Regular curves

2.1.1 Parametrized curves

We want to represent the subsets of $\mathbb{R}^3$ that could be thought as one-dimensional objects ,i.e., the *curves*. To this end we present the following definition

Definition 2.1.1. A parametrized differentiable curve is a map $\boldsymbol{\alpha}$: I $\to \mathbb{R}^3$ of an open interval $I = (a, b)$ of the real line into $\mathbb{R}^3$

The map $\boldsymbol{\alpha}(t) = (x(t), y(t), z(t))$ is said to be differentiable if the functions $x(t), y(t), z(t)$ are differentiable, and $t \in I$ is the parameter. We denote the first derivative as $\boldsymbol{\alpha}'(t) = (x('t), y'(t), z'(t))$ and it known as *tangent vector* or *velocity vector*.

Example 2.1.2. A classical example is the parametrized curve that has as its trace a helix (see Fig. 2.1). Where the parameter t is the angle between the x axis and the line that goes from the origin to the point of projection of the point $\boldsymbol{\alpha}(t)$ in the xy-plane.

$$\boldsymbol{\alpha}(t) = (a\cos(t), a\sin(t), bt), \quad t \in \mathbb{R}$$

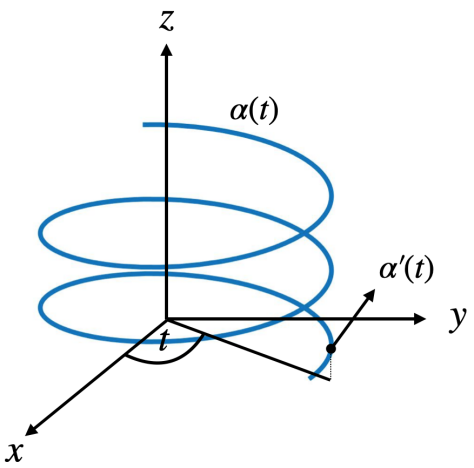

Figure 2.1: The helix.

Another examples of parametrized curves include the ones that have not one-to-one relation, and even we could have two or more curves that have the same trace. We could find these examples in [11] .

The regularity of a curve has a sustantial importance since it allow us to define the arc length and therefore to write a new parametrization for the curves.

Definition 2.1.3. A differentiable curve $\boldsymbol{\alpha}$: I $\to \mathbb{R}^3$ is said to be regular if $|\boldsymbol{\alpha}'(t)| \neq 0$ for all $t \in I$.

Following this definition we have that a *singular point* of $\boldsymbol{\alpha}(t)$ is such that $\boldsymbol{\alpha}'(t) = 0$.

2.1.2 The arc length

Definition 2.1.4. Given a $t \in I$ the *arc length* of a regular parametrized curve $\boldsymbol{\alpha}$: I $\to \mathbb{R}^3$ is

$$s(t) = \int_{t_0}^{t} |\boldsymbol{\alpha}'(t)|dt, \tag{2.1}$$

where $|\boldsymbol{\alpha}'(t)| = \sqrt{(x'(t))^2 + (y'(t))^2 + (z'(t))^2}$ is the length of the vector $\boldsymbol{\alpha}'(t)$.

The arc length is an intrinsic property of a curve and does not depend on the parametrization. To get an idea of this formula, we consider the interval $[c, d]$, s.t., $a < c < d < b$ and we divided it as follows $c = t_0 < t_1 < t_2 < \cdots < t_n = b$. Then we can approximate the arc length as

$$s(t) \approx \sum_{i=1}^{n} ||\boldsymbol{\alpha}(t_{n+1}) - \boldsymbol{\alpha}(t_n)||,$$

Now, if we have a sufficiently large n we can approximate

$$\frac{\boldsymbol{\alpha}(t_{i+1}) - \boldsymbol{\alpha}(t_i)}{t_{i+1} - t_i} \approx \boldsymbol{\alpha}'(t_i),$$

for every i, and substituting in the expression above, we found

$$s(t) \approx \sum_{i=1}^{n} ||\boldsymbol{\alpha}'(t_i)|||t_{i+1} - t_i|,$$

which we can identify with the Riemann sum and lead us to the expression (2.1). A detail proof can be consulted in [12].

As we previously mentioned we could have several curves that have the same trace. In other words we could have several parametrizations for the same curve. In particular we are interested in the parametrization by the length arc. Let us assume we have a parametrized curve $\boldsymbol{\alpha} : I \to \mathbb{R}^3$ we can have also a parametrization $\boldsymbol{\beta} : J \to \mathbb{R}^3$ by the arc length that has the same trace. In fact, since we have that $|\boldsymbol{\alpha}'(t)| \neq 0$ then using the definition (2.1) we observe that $s(t)$ is strictly monotone, which implies that we could find an inverse function $t = t(s) = s^{-1}$, $s \in s(I) = J$. Now if $\boldsymbol{\beta}(s) = \boldsymbol{\alpha} \circ s^{-1}(s)$

$$\boldsymbol{\beta}'(s) = \boldsymbol{\alpha}'(s^{-1}(s))(s^{-1}(s))' = \boldsymbol{\alpha}'(s^{-1}(s))\frac{1}{s'(t)},$$

and by the definition of arc length we find that the velocity vector is $|\boldsymbol{\beta}'(s)| = 1$.

2.1.3 Frenet frame

Since the the main objective is to model the pellicle of the euglena taking into account the elastic properties we should have some physical quantities that will link the deformation with the geometry itself. As we will explore in the next chapter, we need a bit more complex geometric object to construct the final model. Now, we introduce the concepts that will help us to characterize the regular curves.

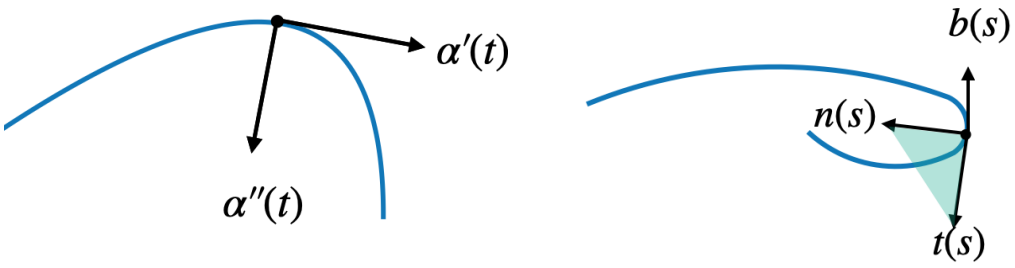

Figure 2.2: Curvature $\boldsymbol{\alpha}''(s)$ normal to the tangent line $\boldsymbol{\alpha}'(s)$(left). Tangent line, normal and binormal vectors at s, shadow area is known as *osculating plane* (right).

Definition 2.1.5. Let $\boldsymbol{\alpha}$: I $\to \mathbb{R}^3$ be a parametrized by the arc length curve $s \in I$ the quantity $|\boldsymbol{\alpha}''(s)| = k(s)$ is called the *curvature* of $\boldsymbol{\alpha}$ at s.

This quantity tell us how rapidly the the curve "pulls away" from the tangent line at s, in a neighbourhood of s. (see Fig. (2.2)) Now, at points where $k(s) \neq 0$ we can define a unit normal vector as $\boldsymbol{\alpha}''(s) = k(s)\boldsymbol{n}(s)$. Let us note that

$$\frac{d}{dt}(\boldsymbol{\alpha}'(s) \cdot \boldsymbol{\alpha}'(s)) = 1$$

$$\Rightarrow 2\boldsymbol{\alpha}''(s) \cdot \boldsymbol{\alpha}'(s) = 0$$

Therefore, $\boldsymbol{\alpha}'(s)$ is normal to $\boldsymbol{n}(s)$. We denote $\boldsymbol{t}(s) = \boldsymbol{\alpha}'(s)$ the tangent vector, therefore $\boldsymbol{t}'(s) = k(s)\boldsymbol{n}(s)$. We define the *binormal vector* $\boldsymbol{b}(s) = \boldsymbol{t}(s) \wedge \boldsymbol{n}(s)$, where "$\wedge$" represents the vector product also known as *cross product*, and it is normal to the osculating plane (see Fig. (2.2)). Similarly to the tangent line, $\boldsymbol{b}'(s)$ measures how rapidly the curve "pulls away" from the osculating plane. Let us note the following

$$\boldsymbol{b}'(s) = \boldsymbol{t}'(s) \wedge \boldsymbol{n}(s) + \boldsymbol{t}(s) \wedge \boldsymbol{n}'(s) = k(s)\boldsymbol{n}(s) \wedge \boldsymbol{n}(s) + \boldsymbol{t}(s) \wedge \boldsymbol{n}'(s)$$

$$\Rightarrow \boldsymbol{b}'(s) = \boldsymbol{t}(s) \wedge \boldsymbol{n}'(s)$$

From here we observe that $\boldsymbol{b}'(s)$ is normal to $\boldsymbol{t}(s)$, thus $\boldsymbol{b}'(s)$ is parallel to $n(s)$, we denote

$$\boldsymbol{b}'(s) = \tau(s)\boldsymbol{n}(s)$$

Definition 2.1.6. Let $\boldsymbol{\alpha}$: I $\to \mathbb{R}^3$ be a parametrized by the arc length curve $s \in I$ the quantity $\tau(s)$ defined by $\boldsymbol{b}'(s) = \tau(s)\boldsymbol{n}(s)$ is called the *torsion* of $\boldsymbol{\alpha}$ at s.

We have that for every value of the parameter s, we have the associated *Frenet frame*, $\boldsymbol{t}(s), \boldsymbol{b}(s), \boldsymbol{n}(s)$, which rules the behaviour of the curve locally. Let us compute $\boldsymbol{n}'(s)$, since $\boldsymbol{n}(s) = \boldsymbol{b}(s) \wedge \boldsymbol{t}(s)$

$$\boldsymbol{n}'(s) = \boldsymbol{b}'(s) \wedge \boldsymbol{t}(s) + \boldsymbol{b}(s) \wedge \boldsymbol{t}'(s) = \tau(s)\boldsymbol{n}(s) \wedge \boldsymbol{t}(s) + \boldsymbol{b}(s) \wedge k(s)\boldsymbol{n}(s)$$

$$\Rightarrow \boldsymbol{n}'(s) = -k(s)\boldsymbol{t}(s) + \tau(s)\boldsymbol{b}(s)$$

We can think that a curve is a combination of bending and twisting. Thus, is will be ruled by the *Frenet formulas*

$$\boldsymbol{t}'(s) = k(s)\boldsymbol{n}(s), \tag{2.2a}$$
$$\boldsymbol{n}'(s) = -k(s)\boldsymbol{t}(s) - \tau(s)\boldsymbol{b}(s), \tag{2.2b}$$
$$\boldsymbol{b}'(s) = -\tau(s)\boldsymbol{n}(s). \tag{2.2c}$$

In equations (2.2) we have adopted the sign convection of [11], but other authors use $-\tau(s)$.

2.2 Regular surfaces

In this section we introduce the concepts and definitions around the regular surfaces along with the first and second fundamental forms, that will help us to make measurements over a surface. In the next chapter we connect these notions with the geometric objects to complete the model.

Definition 2.2.1. A subset $S \subset \mathbb{R}^3$ is a regular surface if for every point $P \in S$, there exists a neighbourhood $V \subset \mathbb{R}^3$ and a map $\mathbf{x} : U \to V$ of an open set $U \subset S$ onto $V \cap S \subset \mathbb{R}^3$ such that

1. $\mathbf{x}$ is differentiable.[1]
2. $\mathbf{x}$ is a homeomorphism.[2]
3. For each $q \in U$ the differential $d\mathbf{x}_q : \mathbb{R} \to \mathbb{R}^3$ is one-to-one.

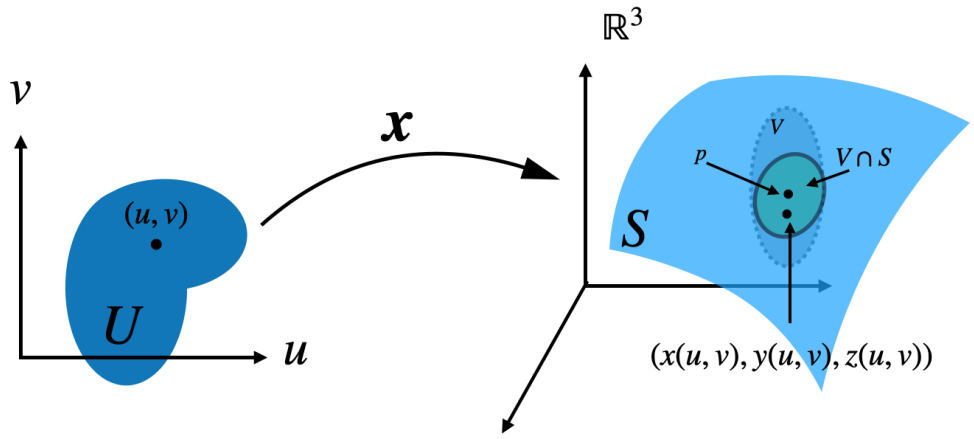

Figure 2.3: Representation of the map $\mathbf{x}$ that defines a regular surface S.

2.2.1 The tangent plane

In order to present the fundamental forms that will complete the brief analysis of the regular curves, we lack the concept of tangent plane. The definition of regular surface guarantees that the set of tangent vectors at $p \in S$ constitutes a plane.

Proposition 2.2.2. *Let $\mathbf{x} : \mathbb{R}^2 \to S$ be a parametrization of a regular surface S and $q \in U$. The vector $d\mathbf{x}_q(\mathbb{R}^2) \subset \mathbb{R}^3$ coincides with the set of tangent vectors to S.*

A detail proof can be seen in [11]. The plane $d\mathbf{x}_q(\mathbb{R}^2)$ that passes through $\mathbf{x}(q)$ will be called *tangent plane*, denoted by $T_p(s)$, and it does not depend on the parametrization. The parametrization $\mathbf{x}$ determines a basis $\{ \frac{\partial \mathbf{x}}{\partial u}, \frac{\partial \mathbf{x}}{\partial v} \}$ of $T_p(s)$. We can also define a normal vector for every point $q \in U$ by

$$\boldsymbol{N}(q) = \frac{\mathbf{x}_u \wedge \mathbf{x}_v}{|\mathbf{x}_u + \mathbf{x}_v|}.$$

2.2.2 First fundamental form

The concept of *first fundamental form* in one of the key concepts that will handle through this work because it allow us to make measurements over a surface, as we explain further below.

Given two vectors $\mathbf{v}, \mathbf{w} \subset \mathbb{R}^3$ we consider the Euclidean inner product $\langle \mathbf{v}, \mathbf{w} \rangle = v_1 w_1 + v_2 w_2 + v_3 w_3$. If $\mathbf{v}, \mathbf{w} \in T_p(S)$, we define

[1] This is that there exists the partial derivatives $\mathbf{x}_u, \mathbf{x}_v$

[2] This means that $\mathbf{x}$ has an inverse $\mathbf{x}^{-1}$which is continuous.

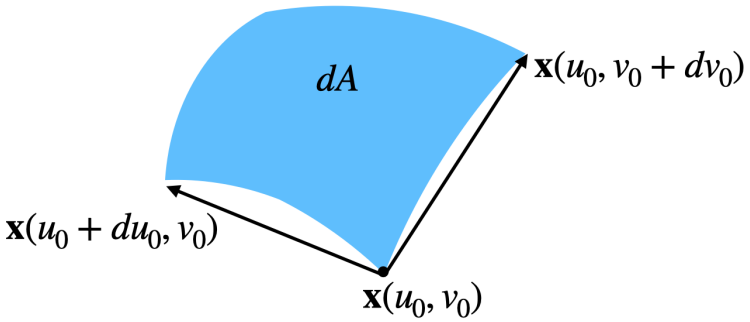

Figure 2.4: Differential of area over a surface.

Definition 2.2.3. The quadratic form,

$$I_p(\mathbf{w}) = \langle \mathbf{w}, \mathbf{w} \rangle = |\mathbf{w}|^2 \geq 0$$

is called the *first fundamental form* $I_p(\mathbf{w})$ on $T_q(S)$ of the regular surface $S \subset \mathbb{R}^3$ at $p \in S$.

Taking the basis $\{\mathbf{x}_u, \mathbf{x}_v\}$ of $T_p(q)$ we can express the vectors as $\mathbf{v} = v_1\mathbf{x}_u + v_2\mathbf{x}_v$, $\mathbf{w} = w_1\mathbf{x}_u + w_2\mathbf{x}_v$ and computing the first fundamental form associated we have

$$\begin{aligned} I_p(\mathbf{w}) &= \langle \mathbf{w}, \mathbf{w} \rangle_p \\ &= \langle \mathbf{x}_u w_1 + \mathbf{x}_v w_2, \mathbf{x}_u w_1 + \mathbf{x}_v w_2 \rangle_p \\ &= \langle \mathbf{x}_u, \mathbf{x}_u \rangle_p (w_1)^2 + 2 \langle \mathbf{x}_u, \mathbf{x}_v \rangle_p w_1 w_2 + \langle \mathbf{x}_v, \mathbf{x}_v \rangle_p (w_2)^2 \\ &= E(w_1)^2 + 2F w_1 w_2 + G(w_2)^2, \end{aligned}$$

or in the matrix form

$$I_p(\mathbf{w}) = \begin{bmatrix} w_1 & w_2 \end{bmatrix} \begin{bmatrix} E & F \\ F & G \end{bmatrix} \begin{bmatrix} w_1 \\ w_2 \end{bmatrix},$$

where we have defined the *coefficients of the first fundamental form*:

$$E = \langle \mathbf{x}_u, \mathbf{x}_u \rangle_p, \tag{2.3a}$$

$$F = \langle \mathbf{x}_u, \mathbf{x}_v \rangle_p = \langle \mathbf{x}_v, \mathbf{x}_u \rangle_p, \tag{2.3b}$$

$$G = \langle \mathbf{x}_v, \mathbf{x}_v \rangle_p. \tag{2.3c}$$

As we mentioned before, we connect the first fundamental form with the local properties of a regular surface. First, we consider a parametrized curve $\boldsymbol{\alpha}(t)$ over a surface S, we know that the arc length is given by

$$s(t) = \int_{t_0}^{t} |\boldsymbol{\alpha}'(t)| dt,$$

if $\boldsymbol{\alpha}(t) = \mathbf{x}(u(t), v(t))$ it is easy to check that the arc length is given by

$$s(t) = \int_{t_0}^{t} \sqrt{E(u')^2 + 2Fu'v' + G(v')^2} dt,$$

We can also compute the area of a bounded region over a surface. To show this, we consider an approximation of the parallelogram with vertices $\mathbf{x}(u_0, v_0)$, $\mathbf{x}(u_0, v_0 + dv_0)$, $\mathbf{x}(u_0 + du_0, v_0)$, $\mathbf{x}(u_0 + du_0, v_0 + dv_0)$ (see Fig. (2.4)). Therefore, we can approximate $dA = |\mathbf{x}_u du \wedge \mathbf{x}_v dv|$. Thus, we define

Definition 2.2.4. Let $R \subset S$ a bounded region of a surface on a neighbourhood of the parametrization $\mathbf{x} : U \subset S \to \mathbb{R}^2$, the quanitity $A(R)$ defined as

$$A(R) = \int_Q |\mathbf{x}_u \wedge \mathbf{x}_v| du dv, \quad Q = \mathbf{x}^{-1}(R),$$

is called the area of R.

It can be proven (see [12]) that

$$det \begin{bmatrix} E & F \\ F & G \end{bmatrix}^2 = EG - F^2 = |\mathbf{x}_u du \wedge \mathbf{x}_v dv|,$$

therefore, the area is related with the coefficients of the first fundamental form as

$$A(R) = \int_Q \sqrt{EG - F^2} du dv,$$

Several examples for computing the coefficients and the mentioned properties can be consulted elsewhere [11, 12, 13].

2.2.3 Second fundamental form

In this section we expose the second fundamental form, that roughly speaking can be consider as the curvature of a regular surface. To this end we need the definition of a Gauss map

Definition 2.2.5. Let $S \in \mathbb{R}^3$ be a regular surface with an orientation[3] $\mathbf{N}$. The map $\mathbf{N} : S \to S^2$, where S^2 is the unit sphere in $\mathbb{R}^3$, is called the Gauss map.

From this definition we notice that the map $\mathrm{d}\mathbf{N}_p : T_p(S) \to T_{N(p)}(S^2)$ takes any parametrized curve $\boldsymbol{\alpha}(t) \in S$, with $\boldsymbol{\alpha}(0) = p$ and map it to a parametrized curve $N \circ \boldsymbol{\alpha}(t) \in S^2$. Noticing that the tangent vector $\mathbf{t} = \mathrm{d}\mathbf{N}_p(\boldsymbol{\alpha}'(0))$ (see Fig. 2.5), we see that $\mathrm{d}\mathbf{N}_p$ measures how much $\mathbf{N}$ pulls away from $\mathbf{N}(p)$ on a neighbourhood of p.
One can prove that the map $\mathrm{d}\mathbf{N}_p : T_p(S) \to T_{N(p)}(S^2)$ is a self-adjoint map (see for instance [11]), and this allow us to associate a quadratic form:

Definition 2.2.6. The quadratic form II_p defined in $T_p(S)$ as,

$$II_p(\mathbf{v}) = -\langle \mathrm{d}\mathbf{N}_p(\mathbf{v}), \mathbf{v} \rangle$$

is called the *second fundamental form* of the regular surface S at $p \in S$.

Similarly to what we did with the first fundamental form, we can take the basis $\{\mathbf{x}_u, \mathbf{x}_v\}$ and express the second fundamental form as

$$\begin{aligned} II_p(\alpha') &= -\left\langle \mathrm{d}\mathbf{N}(\alpha'), \alpha' \right\rangle = -\left\langle \mathbf{N}_u\mathbf{u}' + \mathbf{N}_v\mathbf{v}', \mathbf{x}_u\mathbf{u}' + \mathbf{x}_v\mathbf{v}' \right\rangle \\ &= e(\mathbf{u}')^2 + 2f\mathbf{u}'\mathbf{v}' + g(\mathbf{v}')^2 \end{aligned}$$

where e, f, g are the *coefficients of the second fundamental form*:

$$e = -\langle \mathbf{N}_u, \mathbf{x}_u \rangle, \tag{2.4a}$$
$$f = -\langle \mathbf{N}_u, \mathbf{x}_v \rangle = -\langle \mathbf{N}_v, \mathbf{x}_u \rangle, \tag{2.4b}$$
$$g = -\langle \mathbf{N}_v, \mathbf{x}_v \rangle. \tag{2.4c}$$

Now we present some additional concepts but the reader should consult [14, 15] for a complete deduction and analysis. Considering an orthonormal basis $\{\mathbf{e}_1, \mathbf{e}_2\}$ of $T_p(S)$, the second fundamental form has two extreme values called the principal curvatures restricted to a circle over $T_p(S)$. Then the map $\mathrm{d}\mathbf{N}$ is expressed in terms of these quantities as $\mathrm{d}\mathbf{N}(\mathbf{e}_1) = -k_1\mathbf{e}_1$, $\mathrm{d}\mathbf{N}(\mathbf{e}_2) = -k_2\mathbf{e}_2$. Moreover, we can define the following

[3] It admits a normal field $\mathbf{N}$ over the whole surface

Definition 2.2.7. Let d$\mathbf{N}$ be the differential of the Gaussian map, the determinant of the d$\mathbf{N}$, K, is called the *Gaussian curvature*, and the negative half of the trace of d$\mathbf{N}$, H, is called the *mean curvature*, and they are express in terms of the principal curvatures as

$$K = k_1 k_2, \qquad H = \frac{k_1 + k_2}{2}.$$

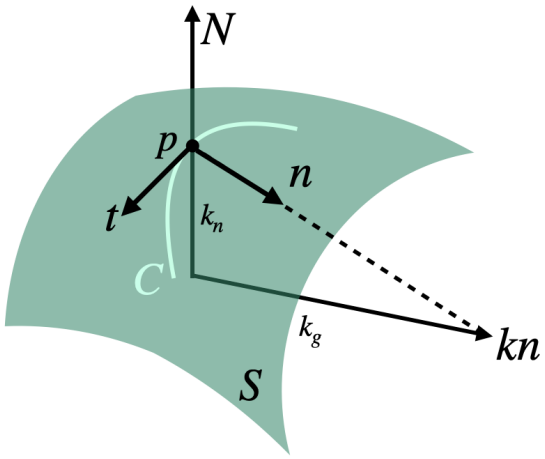

Figure 2.5: Normal and geodesic curvatures.

Let us consider a curve $C \subset S$ over a surface $S \subset \mathbb{R}^3$, we can relate the unit tangent vector $\mathbf{t}$, with the normal tangent vector $\mathbf{n}$ as $\mathbf{k} = \frac{d\mathbf{t}}{ds} = \mathbf{k}_n + \mathbf{k}_g$,where $\mathbf{k}_n$ and $\mathbf{k}_g$ are the normal and geodesic curve vectors, respectively (see Fig.(2.5)).

It is not very useful to present all the relations between the presented geometric properties, but we should mention that all of these concepts will characterize a regular surface. As we move along through this work we may present some specific concepts that we could have not shown yet. We must keep in mind that our main objective is to model the pellicle of the euglena but we lack some geometric objects, those are called rods, these are presented in the next chapter together with some mechanical properties.

Chapter 3

Euglenids pellicle model

In this chapter we are going to present the mathematical model to describe the metaboly, cell movement typically showing a shape shifting, of the euglenids, linking the mechanics of the rods and the surface kinematics as it is proposed in [16, 17]. We proceed to find the energy functional that describes the deformed configuration so we can implement the computational algorithm that minimizes this functional given the boundary conditions.

3.1 Pellicle deformation

The euglenids pellicle is a novel cytoskeleton comprised of parallel proteinaceous strips and microtubules positioned beneath the plasma membrane [9]. Roughly speaking, we can consider the pellicle made of adjacent strips connected between them (see Fig. 3.1). To obtain a mathematical model to describe the kinematics of the pellicle we consider the proteinaceous strips as elastics rods. The elastics rods are elastic slender bodies, this means that their length in one spatial dimension is much greater than the other two. In this section we only present a general description and how we link these with the contiuum model presented in the next section. For a complete theory, see [18].

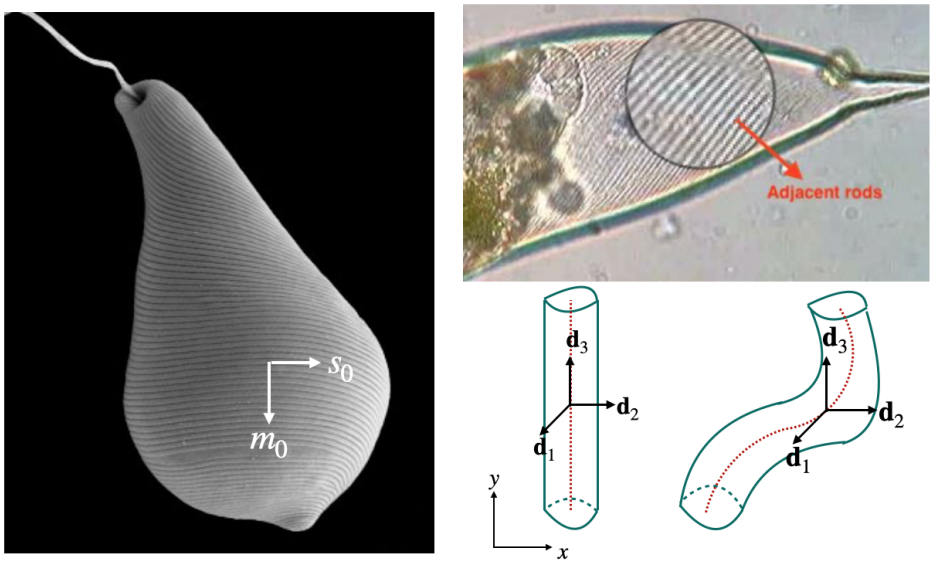

Figure 3.1: Scanning electron micrographs of euglenids pellicle showing the tangent vector field m_0, s_0. Original image taken from The tree of life project, © 2003 Brian S. Leander (left). Euglena pellicle made of adjacent rods. Modify image under the license CC BY-ND 2.0. (upper right). Reference and deformed configurations of a rod (lower right).

Let us consider a reference configuration surface parametrized by $\mathbf{x}_0(u, v)$ and mapped into a deformed configuration parametrized by $\mathbf{x}(u, v) = \sum_{i=1}^{3} x^i \mathbf{e}_i$, then we can write the gradient deformation

tensor using the Cauchy-Green deformation tensor as [19]

$$\boldsymbol{C} = \boldsymbol{F}^T\boldsymbol{F} = \boldsymbol{Id} + \gamma\left(\boldsymbol{s}_0 \otimes \mathbf{x}_0 + \mathbf{x}_0 \otimes \boldsymbol{s}_0\right) + \gamma^2 \mathbf{x}_0 \otimes \mathbf{x}_0,$$

Also, the components of the Cauchy-Green tensor in the basis $\{\boldsymbol{x}_{0,i}, i = u, v\}$, where the comma denotes the partial differentation, are equal to the ones of the metric tensor, and given by the scalars products of the tangent vectors to the deformed surface

$$C_{ij} = g_{ij} = \mathbf{x}_{,i} \cdot \mathbf{x}_{,j}\,.$$

When we consider cylindrical axisymmetric surfaces, we can choose the orientation of the pellicle rods such that, $\mathbf{x}_{0,u} = m_0$ and $\mathbf{x}_{0,v} = s_0$, then a given function $\gamma(u, v)$ that represents the actuation given by pure simple shear should satisfy the non-linear partial differential equations

$$\begin{bmatrix} \mathbf{x}_u \cdot \mathbf{x}_u & \mathbf{x}_u \cdot \mathbf{x}_v \\ \mathbf{x}_u \cdot \mathbf{x}_v & \mathbf{x}_v \cdot \mathbf{x}_v \end{bmatrix} = \begin{bmatrix} 1+\gamma^2 & \gamma \\ \gamma & 1 \end{bmatrix}.$$

The Gaussian curvature of the target metric can be obtain by differentiating the metric tensor, as it is explained in [11] as

$$K = (\gamma_{,v} - \gamma\gamma_{,u})_{,u}.$$

We proceed to analyze the mechanics of the rods so we can finally write down the energy functional and obtain the computational model.

3.2 Mechanics of rods

In order to describe the deformation of the rod we consider the following. First, we consider a reference configuration at a time t_0, and evolves into a deformed configuration at time t (see Fig. (3.1)). Moreover, we consider a centre line (dashed line) that is parallel to the z coordinate, it is denoted by s. Now, to track the twist and bending we consider the material frame $(\mathbf{d}_1, \mathbf{d}_2, \mathbf{d}_3)$, this frame it is considered to be orthogonal under small deformations and it is attached to the centre line. The centre line and the triad constitute a *Cosserat curve*.

We make the following assumptions:

- The rods has uniform properties along its length. All cross-sections are identical
- Under uniform or small strain, the material frame deforms in a rigid manner when we vary s.

From these assumptions, it can be proven that the material frame satisfies the following equations

$$\mathbf{d}_1'(s) = \tau(s)\mathbf{d}_2(s) - \kappa^{(2)}(s)\mathbf{d}_3(s) \tag{3.1a}$$

$$\mathbf{d}_2'(s) = -\tau(s)\mathbf{d}_1(s) + \kappa^{(1)}(s)\mathbf{d}_3(s) \tag{3.1b}$$

$$\mathbf{d}_3'(s) = \kappa^{(2)}(s)\mathbf{d}_1(s) - \kappa^{(1)}(s)\mathbf{d}_2(s) \tag{3.1c}$$

We can immediately note the similarity with the Frenet equations presented in the previous chapter. The functions $\kappa^{(1)}(s), \kappa^{(2)}(s)$ represent how much the material frame rotates around $\mathbf{d}_1$ and $\mathbf{d}_2$, respectively (bending in plane and out-of-plane). The function $\tau(s)$ represents how much the material frame rotates around the tangent $\mathbf{d}_3$ (twist). These equations can be rewritten in terms of the *Darboux vector*, $\boldsymbol{\Omega}(s)$ as

$$\mathbf{d}_1'(s) = \boldsymbol{\Omega}(s) \times \mathbf{d}_1, \quad \mathbf{d}_2'(s) = \boldsymbol{\Omega}(s) \times \mathbf{d}_2, \quad \mathbf{d}_3'(s) = \boldsymbol{\Omega}(s) \times \mathbf{d}_3$$

where $\boldsymbol{\Omega}(s) = \kappa^{(1)}(s)\mathbf{d}_1(s) + \kappa^{(2)}(s)\mathbf{d}_2(s) + \tau(s)\mathbf{d}_3(s)$ represents the total rate of rotation per unit length along the centre line.

At this point, we lack the relation between the surface and the rods, which complete the pellicle model. This is presented in the following section where symmetric considerations are made.

3.3 Continuum model of euglenids pellicle

We can consider a continuum model of the euglenids pellicle since this is made of few tens of adjacent rods, as reported in [19]. The metaboly is assumed to be produced by simple shear along the pellicle strips. Our main goal is to create a continuum model of the pellicle surface linking the rods kinematics to the surface kinematics. To this end we present the following approach.

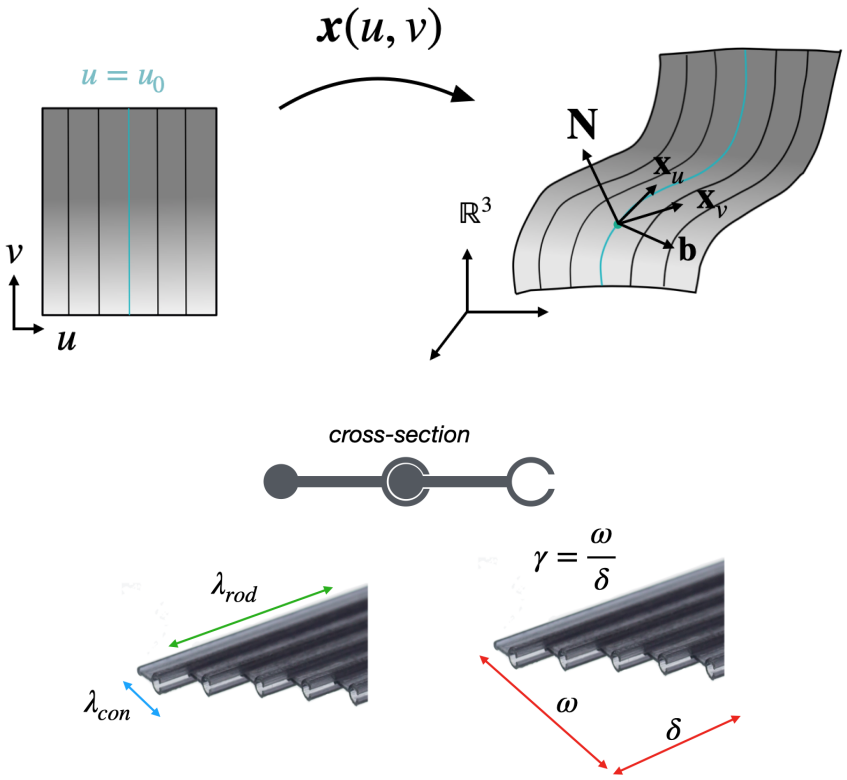

Figure 3.2: Reference configuration (left) mapped into a deformed configuration (right)

Let us assume a reference configuration that is mapped through $\mathbf{x}(u, v)$ into a deformed configuration as it is shown in the figure (3.2). We assume that the rods are aligned with the v coordinate in the reference configuration. In the deformed configuration we have the normal vector to the surface, defined as before

$$\boldsymbol{N} = \frac{\mathbf{x}_u \wedge \mathbf{x}_v}{|\mathbf{x}_u + \mathbf{x}_v|}.$$

We introduce a unit tangent vector to the surface defined as

$$\begin{aligned}\mathbf{b} &= \frac{1}{|\mathbf{x}_v|}\mathbf{x}_v \wedge \mathbf{N} = \frac{1}{|\mathbf{x}_v|\,|\mathbf{x}_u \wedge \mathbf{x}_v|}\mathbf{x}_v \wedge (\mathbf{x}_u \wedge \mathbf{x}_v) \\ &= \frac{1}{\sqrt{G}\sqrt{EG - F^2}}\left(G\mathbf{x}_u - F\mathbf{x}_v\right).\end{aligned}$$

As we can see in the Fig.(3.2), the stretch of the connectors λ_{con}, i.e., the projection of the $\mathbf{x}_u$ along the vector $\mathbf{b}$ and the stretch of the rods λ_{rod} are given by

$$\lambda_{con} = \mathbf{x}_u \cdot \mathbf{b} = \frac{\sqrt{EG - F^2}}{\sqrt{G}} = \sqrt{E - F^2/G},$$

$$\lambda_{rod} = |\mathbf{x}_v| = \sqrt{G}.$$

Where we keep the notation of [11] for the coefficients of the first fundamental form. Let us note that if we impose the inextensibility of rods, that is, $G = 1$, the inextensibility of connectors $\lambda_{con} = 1$ is equivalent to the area conservation, since $\sqrt{EG - F^2} = 1$.
We have that the surface is made of adjacent rods, therefore we assume that the material frame $(\mathbf{d}_1, \mathbf{d}_2, \mathbf{d}_3)$ can be expressed as follows

$$\mathbf{d}_1 = \mathbf{N}, \quad \mathbf{d}_2 = \mathbf{b}, \quad \mathbf{d}_3 = \frac{\mathbf{x}_v}{|\mathbf{x}_v|}.$$

Now, let us note that if we take the equations (3.1), and assume that the material frame remains almost orthonormal, that is $\mathbf{d}_i \cdot \mathbf{d}_j = 0$, we can write the rods strains $\kappa^{(1)}, \kappa^{(2)}, \tau$ as

$$\kappa^{(1)} = -\mathbf{d}_3' \cdot \mathbf{d}_2, \quad \kappa^{(2)} = \mathbf{d}_3' \cdot \mathbf{d}_1, \quad \tau = \mathbf{d}_1' \cdot \mathbf{d}_2.$$

where the notation " $(\cdot)'$ " represents the partial derivative with respect to the parameter v. This can also be seen if we consider the covariant derivative that is the projection of the $\mathbf{d}_3'$ onto the plane spaned by $\mathbf{d}_1, \mathbf{d}_2$

$$\frac{D\mathbf{d}_3}{dv} = \left(\mathbf{d}_3' \cdot \mathbf{d}_2\right)\mathbf{d}_2 + \left(\mathbf{d}_3' \cdot \mathbf{d}_3\right)\mathbf{d}_3 = \left(\mathbf{d}_3' \cdot \mathbf{d}_2\right)\mathbf{d}_2,$$

since $\mathbf{d}_3 \cdot \mathbf{d}_3 = 1$. It can be proven that the rod strains $\kappa^{(1)}, \kappa^{(2)}$ are the geodesic and the normal curvatures respectively.
From this equations we can compute the rod strains and we get

$$\begin{aligned}
\kappa^{(1)} &= \frac{1}{\sqrt{EG - F^2}}(-\mathbf{x}_u \cdot \mathbf{x}_{vv} + \frac{F}{G}\mathbf{x}_v \cdot \mathbf{x}_{vv}), \\
\kappa^{(2)} &= \frac{\mathbf{x}_{vv} \cdot \mathbf{N}}{\sqrt{G}} = \frac{g}{\sqrt{G}}, \\
\tau &= \frac{1}{\sqrt{G}\sqrt{EG - F^2}}(-G\mathbf{N} \cdot \mathbf{x}_{uv} + F\mathbf{N} \cdot \mathbf{x}_{vv}) = \frac{1}{\sqrt{G}\sqrt{EG - F^2}}(Fg - Gf)
\end{aligned}$$

Additionally we compute the strain associated to the connectors along the direction given by $\mathbf{b}$ using the second fundamental form

$$\kappa_{con} = II_p(\mathbf{b}) = -\left\langle \mathrm{d}\mathbf{N}, \mathbf{b} \right\rangle = \frac{eG^2 - 2fFG + gF^2}{G(EG - F^2)}.$$

We have the necessary elements to characterize the deformed surface. We only lack the parametrization that is consider in the following section.

3.3.1 Axisymmetric cylindrical surfaces

The analysis that we present here is done by considering only axisymmetric cylindrical surfaces because they give a wide variety of shapes and have great potential to model several situations of the euglenids metaboly. The main difference with respect the following section is that in here we consider that the connectors could stretch, causing the shape shifting to be more complex.

For this particular surfaces we have the following parametrization [19]

$$\mathbf{x}(u, v) = \begin{pmatrix} r(v)\cos\left(\frac{u}{R_0} + \psi(v)\right) \\ r(v)\sin\left(\frac{u}{R_0} + \psi(v)\right) \\ z(v) \end{pmatrix},$$

where $v = (0, L_0), u = (0, 2\pi R_0)$. From this parametrization we can find all the coefficients of the first and second fundamental form by direct calculations using Eqs. (2.3),(2.4). We obtain

$$E = \left(\frac{r}{R_0}\right)^2, \quad F = \frac{r^2\psi'}{R_0}, \quad G = r'^2 + \left(r\psi'\right)^2 + z'^2 \tag{3.2a}$$

$$e = -\frac{rz'}{R_0^2\sqrt{r'^2+z'^2}}, \quad f = -\frac{r\psi' z'}{R_0\sqrt{r'^2+z'^2}}, \quad g = \frac{z'\left(r'' - r\psi'^2\right) - r'z''}{\sqrt{r'^2+z'^2}} \tag{3.2b}$$

$$m = \mathbf{x}_u \cdot \mathbf{x}_{vv} = \frac{r}{R_0}\left(r\psi'' + 2r'\psi'\right), \quad n = \mathbf{x}_v \cdot \mathbf{x}_{vv} = r'r'' + z'z'' + r\psi'\left(r\psi'' + r'\psi'\right) \tag{3.2c}$$

Using the above results it is possible to write down the elastic energy as a superposition of the bending and twist of the rods and the connectors

$$\begin{aligned} E[\mathbf{x}] = \rho \int_{\Omega_0} \Bigg[& \frac{K_{\text{rod}}}{2}\left(\lambda_{\text{rod}} - 1\right)^2 + \frac{K_{\text{con}}}{2}\left(\lambda_{\text{con}} - 1\right)^2 \\ & + \frac{B_1}{2}\left(\kappa^{(1)} - \kappa^{(1)*}\right)^2 + \frac{B_2}{2}\left(\kappa^{(2)} - \kappa^{(2)*}\right)^2 + \frac{T}{2}\left(\tau - \tau^*\right)^2 + \frac{B_{\text{con}}}{2}\left(\kappa_{\text{con}} - \kappa^*_{\text{con}}\right)^2 \Bigg] dudv \end{aligned} \tag{3.3}$$

where $\Omega_0 = [0, L_0] \times [0, 2\pi R_0]$ and the $\kappa^{(1)*}, \kappa^{(2)*}, \tau^*, \kappa^*_{\text{con}}$ are spontaneous rod strains.
If we compare the energy functional with the one followed by [18], we note that the constants B_1, B_2 are related with the denominated moments of inertia, that are given by

$$I^{(1)} = \int_{\mathcal{D}} (y - y_0) dxdy, \quad I^{(2)} = \int_{\mathcal{D}} (x - x_0) dxdy.$$

where $\mathcal{D}$ is the area of the cross-section. They represent how the centre line of the rods is deformed under some strains. For a circular cross-section, this value is expressed as

$$I^{(1)} = I^{(2)} = \frac{\pi r^4}{4}.$$

The following section explains how the model could be reduced to make our algorithm more efficient.

3.3.2 Reduce model: inextensible rods

The inextensibility of rods and connectors can be model taking the limit $\rho K_{con}, \rho K_{rod} \to \infty$ in the Eq. (3.3), from this will obtain the new expressions for the coefficients of the first form

$$E = 1 + \gamma^2, \quad F = \gamma, \quad G = 1.$$

This reduction permits to express the parametrization in terms of $\gamma(v)$ only as

$$r = R_0\sqrt{1+\gamma^2}, \quad \psi' = \frac{\gamma}{R_0\left(1+\gamma^2\right)}, \quad z' = \sqrt{\frac{1 - \left(R_0\gamma\gamma'\right)^2}{1+\gamma^2}}. \tag{3.4}$$

As we did previously we compute the coefficients (e, f, g, m, n) in terms of $\gamma(v)$ and we obtain

$$e = -\frac{1}{R_0}\sqrt{\left(1 - \left(R_0\gamma\gamma'\right)^2\right)\left(1+\gamma^2\right)},$$

$$f = -\frac{\gamma}{R_0}\sqrt{\frac{1 - \left(R_0\gamma\gamma'\right)^2}{1+\gamma^2}},$$

$$g = \frac{R_0^2\gamma'^2(\gamma^4 + \gamma^2 + 1) + R_0^2\gamma''(\gamma^3 + \gamma) - \gamma^2}{R_0\sqrt{(1 - (R_0\gamma\gamma')^2)(1+\gamma^2)^3}},$$

$$m = -\gamma', \quad n = 0.$$

Let us note that in this limit the energy contributions due to the connectors does not exists, therefore the elastic energy is

$$E[\gamma, \gamma', \gamma''] = \rho \int_{\Omega_0} \left[\frac{B_1}{2} \left(\kappa^{(1)} - \kappa^{(1)*} \right)^2 + \frac{B_2}{2} \left(\kappa^{(2)} - \kappa^{(2)*} \right)^2 + \frac{T}{2} \left(\tau - \tau^* \right)^2 \right] dudv$$

This is a reduce model since we only have the energy functional in terms of $\gamma, \gamma', \gamma''$ instead of r, ψ, z and their derivatives. To use the computational model we have to find the first variation of this functional, the procedure can be seen in Appendix A. From this first variation it is also possible to obtain the Euler-Lagrange equations, but this remains for future work.
In the following section we explore the above models and discuss the results.

Chapter 4

Results

The computational model that we implement works as follows. We consider only inextensible surfaces but using the complete model (in terms of r, ψ, z) and the reduce model (in terms of γ only). For the first one, we write down the energy functional (see Eq. (3.3)) and its first variation in terms of the r, ψ, z and their derivatives that are interpolated using B-splines [20], sufficiently smooth functions so we can compute their derivatives, this is

$$r^h(v) = \sum_{i=1}^{n} B_i(v) r_i, \quad \psi^h(v) = \sum_{i=1}^{n} B_j(v) \psi_j, \quad z^h(v) = \sum_{i=1}^{n} B_k(v) z_k.$$

Afterwards we compute the geometric configuration that allows to minimize this functional using a pre-built MATLAB function called `fminunc()`. We apply a set of boundary conditions: *a*) increase the basal radius, *b*) compressing the cylinder from the top, *c*) compressing the cylinder from both the top and base, *d*) increase both the basal and top radius. The numerical integration to obtain the total energy is done by a quadrature rule. We obtain a wide variety of configurations that are shown in Fig. (4.1).

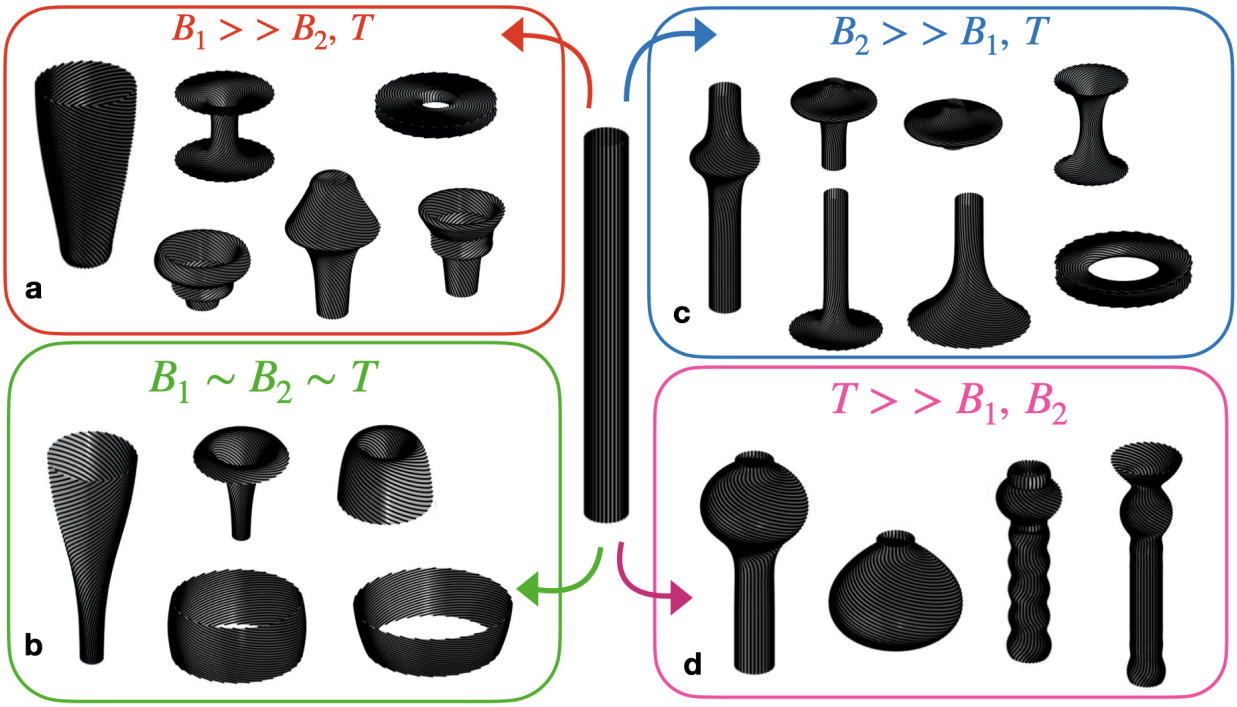

Figure 4.1: Shape configurations for axisymmetric cylindrical surfaces. Fig. (a) shows the model using the parameter values $B_1 = 100,\ B_2 = 1,\ T = 1$. (b) uses the parameter values $B_1 = 1,\ B_2 = 100,\ T = 1$, (c) $B_1 = 1,\ B_2 = 2,\ T = 1$, and (d) $B_1 = 1,\ B_2 = 1,\ T = 100$.

In order to analyze the kinematics behaviour we vary the parameter values B_1, B_2, T. Several shape configurations are obtain varying this parameters as it is shown in Fig. (4.1). Let us note that the case $T >> B_1, B_2$ gave us some shape configurations that are not realistic, since has abrupt changes in the surfaces. In Fig. (4.2) we observe the pellicle kinematics for the cases $B_1 >> B_2, T$, and $B_1 \sim B_2 \sim T$. For the first one we observe smooth transitions between all the configurations (4.2) (a)-(b), meanwhile for the second one (4.2)(c)-(d) we note that some of the transitions are not smooth. A new problem arises, given two known stable states and we want to know the transition between them. One possibility to solve this concern is to use the Nudged Elastic Band (NEB) algorithm [21] to find the smooth transition between the possible states but this will remain as a future work.

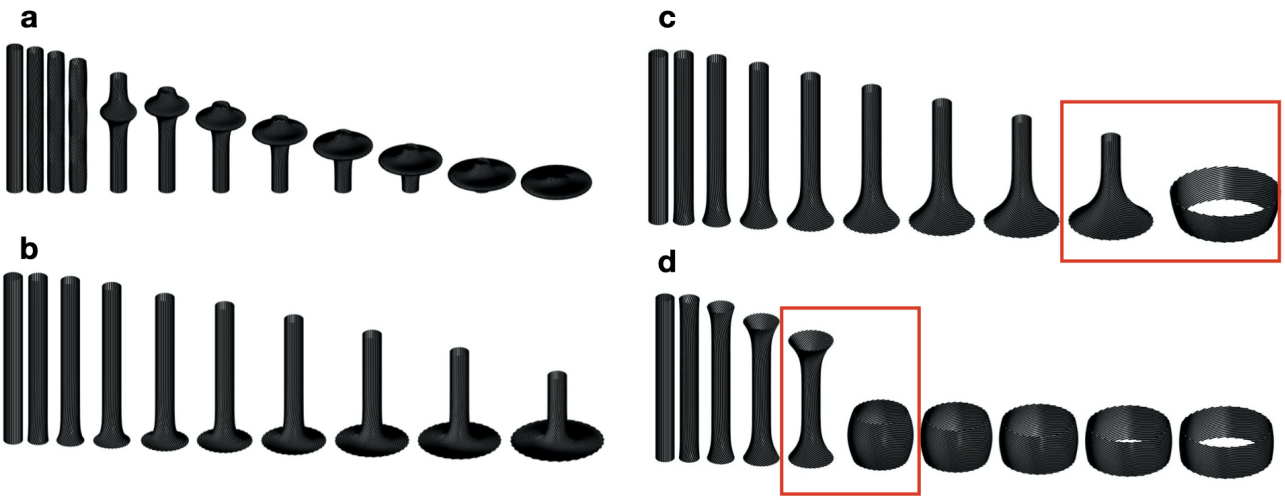

Figure 4.2: Pellicle kinematics for parameter values $B_1 = 100,\ B_2 = 1,\ T = 1$ (left) $B_1 = 1,\ B_2 = 2,\ T = 1$ (right). Figures (b)-(c) correspond to compress top and base, and (a)-(d) to increase basal radius.

The case of the reduce model is explained right below. Let us note that from our consideration of only axisymmetric surfaces $\gamma = \gamma(v)$, we have that the Gaussian curvature is given by

$$K = -(\gamma\gamma_{,v})_{,v}$$

and we can distinguish the cases: $\gamma = const \Rightarrow K = 0$ that produces cylindrical surfaces, $\gamma\gamma_{,v} = const \Rightarrow K = 0$ that produces cones and annuli and $\gamma\gamma_{,v} \neq const \Rightarrow K \neq 0$ producing spheres and pseudospheres as in [19].

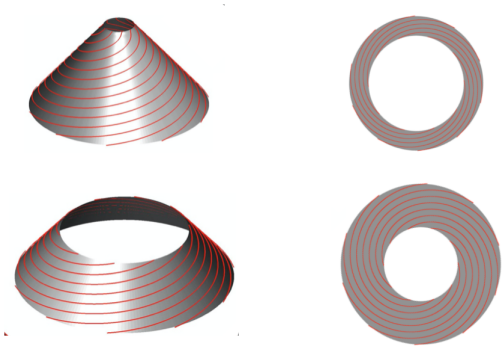

Figure 4.3: Cones and flat annular regions using the square-root dependence in the actuation shear γ.

In this case we only consider the square-root dependence for the actuation shear, that is

$$\gamma(v) = \sqrt{A(1 - u/L_0) + Bu/L_0}$$

that results in cones and flat annular regions. The constants $A, B \geq 0$ have to satisfy the embeddability condition

$$|B - A| \leq \frac{2L_0}{R_0}.$$

From Eq.(3.4) it is easy to check that the quantity $z'(v)/r'(v)$ is independent of u, which leads to truncated cones, as the ones shown in (4.3).
Finally, we compare the two models by computing the total energy in each case which remains the same for a wide range of parameter values. We lack some analysis and comparison between the two models by exploring a wider range of actuation shear, leading to the whole family classified as in [19].

Chapter 5

Conclusions

In this work we link the geometrical properties of the euglenids surface and the mechanics of the rods via the first and second fundamental forms and Crosserat curve. We model the euglenids' pellicle kinematics by proposing a continuum model and considering axisymmetric cylindrical inextensible surfaces with pure simple shear actuation. This results in a wide variety of shape configurations according to the specific types of boundary conditions. The inextensibility of rods let us to make a reduction of the model improving the algorithm efficiency.

Several aspects remains open to explore, such as the variety of actuation shear to construct a larger family of surfaces [19, 16]. We also can study the transitions between states by the use of some algorithm to minimize the energy functional, for instance the NEB [21].
3D printed models based on computational results can be obtain to give a step forward to the implementation of soft robotics and novel mechanisms inspired by this shape morphing mechanism of euglenids [5, 6, 8].

Some fundamental aspects about why the euglenids have this shape shifting mechanism remains unclear, some studies [16, 17] analyze the metaboly by linking the local actuation by the pellicle shear with the shape control. Even recently has been shown that crawling is ruled by the confinement [22] deeper analysis needs to be done to understand this particular and highly intriguing metaboly of these unicellular organisms. In general lots of fundamental questions have to be explore to understand the physics of life.

Appendix A

First variation of energy

The computational algorithm requieres the energy functional as well as their first variation form in order to find the configuration that minimizes Eq. (3.3). In here we present the deduction of the first variaton for the reduce model. From here we can obtain also the Euler-Lagrange equations but this remains as future work.
The first variation of the total energy $\Pi(\gamma)$ is

$$\delta\Pi(\gamma) = \int \left(\frac{\partial E}{\partial \gamma}\tilde{\gamma} + \frac{\partial E}{\partial \gamma'}\tilde{\gamma}' + \frac{\partial E}{\partial \gamma''}\tilde{\gamma}'' \right) dv \tag{A.1}$$

We have to calculate each of this terms. For the first term we have that

$$\frac{\partial E}{\partial \gamma} = \frac{\partial E}{\partial \kappa^{(1)}}\frac{d\kappa^{(2)}}{d\gamma} + \frac{\partial E}{\partial \kappa^{(2)}}\frac{d\kappa^{(2)}}{d\gamma} + \frac{\partial E}{\partial \tau}\frac{d\tau}{d\gamma} = B_1(\kappa^{(1)} - \kappa^{(1)*})\frac{d\kappa^{(1)}}{d\gamma} + B_2(\kappa^{(2)} - \kappa^{(2)*})\frac{d\kappa^{(2)}}{d\gamma} + T(\tau - \tau*)\frac{d\tau}{d\gamma}$$

Then we compute

$$\frac{d\kappa^{(1)}}{d\gamma} = 0,$$

$$\begin{aligned}\frac{d\kappa^{(2)}}{d\gamma} = \frac{dg}{d\gamma} = {} & \frac{1}{R_0}\left(1 - \left(R_0\gamma\gamma'\right)^2\right)^{-1/2}\left(1+\gamma^2\right)^{-3/2}\left[R_0^2\left(4\gamma^3\gamma'^2 + 3\gamma^2\gamma'' + \gamma'' + 2\gamma\gamma'^2\right) - 2\gamma\right] \\ & + \frac{1}{R_0}\left[R_0^2\gamma'^2\gamma\left(1 - \left(R_0\gamma\gamma'\right)^2\right)^{-3/2}\left(1+\gamma^2\right)^{-3/2} - 3\gamma\left(1+\gamma^2\right)^{-5/2}\left(1 - \left(R_0\gamma\gamma'\right)^2\right)^{-1/2}\right] \\ & \left(R_0^2(\gamma^4\gamma'^2 + \gamma^3\gamma'' + \gamma\gamma'' + \gamma^2\gamma'^2 + \gamma'^2) - 2\gamma\right),\end{aligned}$$

An alternate form of $\frac{dg}{d\gamma}$ is

$$\begin{aligned}\frac{dg}{d\gamma} = {} & \frac{1}{R_0(\gamma^2+1)^{5/2}(1-(R_0\gamma\gamma')^2)^{3/2}}\Big[\gamma''(R_0^4\gamma^6\gamma'^2 + R_0^4\gamma^4\gamma'^2 + R_0^2\gamma^2 + R_0^2) \\ & - \gamma^5(R_0^4\gamma'^4 + R_0^2\gamma'^2) + \gamma^3(3R_0^4\gamma'^4 + 4R_0^2\gamma'^2 + 1) + \gamma(R_0^4\gamma'^4 - R_0^2\gamma'^2 - 2)\Big]\end{aligned}$$

$$\frac{d\tau}{d\gamma} = g + \gamma\frac{dg}{d\gamma} - \frac{df}{d\gamma},$$

The remaining term to compute is

$$\frac{df}{d\gamma} = \frac{\left(1 - (R_0\gamma\gamma')^2\right)^{1/2}}{R_0\left(1+\gamma^2\right)^{1/2}}\left[\frac{R_0^2\gamma'^2\gamma^2}{1-(R_0\gamma\gamma')^2} + \frac{\gamma^2}{1+\gamma^2} - 1\right].$$

For the second term we have that

$$\frac{\partial E}{\partial \gamma'} = \frac{\partial E}{\partial \kappa^{(1)}}\frac{d\kappa^{(1)}}{d\gamma'} + \frac{\partial E}{\partial \kappa^{(2)}}\frac{d\kappa^{(2)}}{d\gamma'} + \frac{\partial E}{\partial \tau}\frac{d\tau}{d\gamma'}$$

$$\begin{aligned}
\frac{d\kappa^{(1)}}{d\gamma'} =& -1 \\
\frac{d\kappa^{(2)}}{d\gamma'} = \frac{dg}{d\gamma'} =& \frac{2}{R_0}\left[R_0^2(\gamma^4\gamma' + \gamma^2\gamma' + \gamma')\right]\left[(1-(R_0\gamma\gamma')^2)^{-1/2}(1+\gamma^2)^{-3/2}\right] \\
&+ \frac{1}{R_0}\left[R_0^2\gamma'\gamma^2\left(1-\left(R_0\gamma\gamma'\right)^2\right)^{-3/2}\left(1+\gamma^2\right)^{-3/2}\right]\left[R_0^2(\gamma^4\gamma'^2 + \gamma^3\gamma'' + \gamma\gamma'' + \gamma^2\gamma'^2 + \gamma'^2) - \gamma^2\right] \\
\frac{df}{d\gamma'} =& \frac{R_0\gamma^3\gamma'}{\sqrt{(1-(R_0\gamma\gamma')^2)(1+\gamma^2)}}
\end{aligned}$$

An alternate form of $\frac{dg}{d\gamma'}$ is

$$\frac{dg}{d\gamma'} = -\frac{R_0\gamma'\left[R_0^2\gamma^6\gamma'^2 - R_0^2\gamma^5\gamma'' + \gamma^4(R_0^2\gamma'^2 - 1) - R_0^2\gamma^3\gamma'' + \gamma^2(R_0^2\gamma'^2 - 2) - 2\right]}{(\gamma^2+1)^{3/2}(1-(R_0\gamma\gamma')^2)^{3/2}}$$

For the third term we have that

$$\frac{\partial E}{\partial \gamma''} = \frac{\partial E}{\partial \kappa^{(1)}}\frac{d\kappa^{(1)}}{d\gamma''} + \frac{\partial E}{\partial \kappa^{(2)}}\frac{d\kappa^{(2)}}{d\gamma''} + \frac{\partial E}{\partial \tau}\frac{d\tau}{d\gamma''}$$

$$\begin{aligned}
\frac{d\kappa^{(1)}}{d\gamma''} =& 0 \\
\frac{d\kappa^{(2)}}{d\gamma''} = \frac{dg}{d\gamma''} =& \frac{1}{R_0}\left[R_0^2(\gamma+\gamma^3)\right](1-(R_0\gamma\gamma')^2)^{-1/2}(1+\gamma^2)^{-3/2} = \frac{R_0\gamma}{\sqrt{(1-(R_0\gamma\gamma')^2)(1+\gamma^2)}} \\
\frac{d\tau}{d\gamma''} =& \frac{d}{d\gamma''}(\gamma g - f) = \gamma\frac{dg}{d\gamma''} - \frac{df}{d\gamma''}(=0) = \gamma\frac{d\tau}{d\gamma''}
\end{aligned}$$

Using the expressions above we obtain the first variation Eq.(A.1) and then we proceed to use the computational model to obtain the shape configuration. The Euler-Lagrange equations can be obtained by solving

$$\left.\frac{\partial \Pi(\hat{\gamma})}{\partial \epsilon}\right|_{\epsilon=0} = 0$$

where $\hat{\gamma} = \gamma + \epsilon\tilde{\gamma}$.

Bibliography

[1] Maddison, D. R. and K.-S. Schulz, "The tree of life web project." http://tolweb.org, 2007. Accessed: 2020-09-01.

[2] C. K. Rosenthal, "(1595) invention of the microscope," *Nature Cell Biology*, vol. Milestones in Light Microscopy, no. 1, pp. 1–2, 2009.

[3] E. M. Purcell, "Life at low reynolds number," *American Journal of Physics*, vol. 45, no. 1, pp. 3–11, 1977.

[4] F. Alouges, A. DeSimone, and A. Lefebvre, "Optimal strokes for axisymmetric microswimmers," *The European Physical Journal E*, vol. 28, no. 3, pp. 279–284, 2009.

[5] K. M. Digumarti, *Euglenoid Movement and Novel Mechanisms for Soft Robots*. PhD thesis, University of Bristol, Bristol, UK, Mar. 2019.

[6] K. Digumarti, A. Conn, and J. Rossiter, "Eumobot: replicating euglenoid movement in a soft robot," *Journal of The Royal Society Interface*, vol. 15, p. 20180301, 11 2018.

[7] T. Suzaki and R. Williamson, "Reactivation of euglenoid movement and flagellar beating in detergent-extracted cells of astasia longa: different mechanisms of force generation are involved," *Journal of Cell Science*, vol. 80, no. 1, pp. 75–89, 1986.

[8] K. M. Digumarti, A. Conn, and J. Rossiter, "Euglenoid-inspired giant shape change for highly deformable soft robots," *IEEE Robotics and Automation Letters*, vol. 2, pp. 2302–2307, 2017.

[9] B. S. Leander and M. A. Farmer, "Comparative morphology of the euglenid pellicle. i. patterns of strips and pores," *The Journal of eukaryotic microbiology*, vol. 47, no. 5, p. 469–479, 2000.

[10] Q. Han and J.-X. Hong, *Isometric Embedding of Riemannian Manifolds in Euclidean Spaces*. American Mathematical Society, 2006.

[11] M. P. do Carmo, *Differential Geometry of Curves and Surfaces*. Prentice-Hall, Inc. Englewood Cliffs, 1976.

[12] T. Shrifin, *Differential Geometry: A First Course in Curves and Surfaces*. University of Georgia, 2016.

[13] N. Patrikalakis, T. Maekawa, and W. Chon, *Shape Interrogation for Computed Aided Design and Manufacturing*. Hyperbook Edition, MIT, 2009.

[14] J.-D. Boissonnat and M. Teillaud, *Effective computational geometry for curves and surfaces*. Springer, 2007.

[15] V. A. Toponogov, *Differential geometry of curves and surfaces: A concise guide*. Birkhauser, 2006.

[16] G. Noselli, M. Arroyo, and A. DeSimone, "Smart helical structures inspired by the pellicle of euglenids," *Journal of the Mechanics and Physics of Solids*, vol. 123, pp. 234 – 246, 2019. The N.A. Fleck 60th Anniversary Volume.

[17] M. Arroyo, L. Heltai, D. Millán, and A. DeSimone, "Reverse engineering the euglenoid movement," *Proceedings of the National Academy of Sciences*, vol. 109, no. 44, pp. 17874–17879, 2012.

[18] B. Audoly and Y. Pomeau, *Elasticity and Geometry: From hair curls to non-linear response of shells*. Oxford University Press, 2010.

[19] M. Arroyo and A. DeSimone, "Shape control of active surfaces inspired by the movement of euglenids," *Journal of the Mechanics and Physics of Solids*, vol. 62, pp. 99 – 112, 2014. Sixtieth anniversary issue in honor of Professor Rodney Hill.

[20] K. Höllig, *Finite element methods with B-splines*. Society Industrial and Applied Mathematics, 2003.

[21] G.-R. Qian, X. Dong, X.-F. Zhou, Y. Tian, A. R. Oganov, and H.-T. Wang, "Variable cell nudged elastic band method for studying solid–solid structural phase transitions," *Computer Physics Communications*, vol. 184, no. 9, pp. 2111 – 2118, 2013.

[22] G. Noselli, A. Beran, M. Arroyo, and A. DeSimone, "Swimming euglena respond to confinement with a behavioural change enabling effective crawling," *Nature Physics*, vol. 15, no. 5, pp. 496–502, 2019.